https://doi.org/10.26599/FRICT.2025.9441205

Research Article

# Tribological behavior and lubrication mechanisms of a-C:H films in vacuum from -200 to 25 °C

Yongqi Zhu [a,b], Xiangyu Zong [c], Hongxuan Li [a,b], Pengfei Ju[d], Jingzhou Liu[d], Shunbo Wang [c], Li Ji [a,b,*], Xiaohong Liu [a], Huidi Zhou [a,b], Jianmin Chen [a,b]

[a]*State Key Laboratory of Solid Lubrication, Lanzhou Institute of Chemical Physics, Chinese Academy of Sciences, Lanzhou 730000, China*

[b]*Center of Materials Science and Optoelectronics Engineering, University of Chinese Academy of Sciences, Beijing 100049, China*

[c]*School of Mechanical & Aerospace Engineering, Jilin University, Changchun, 130025, China*

[d]*Shanghai Aerospace Equipment Manufacturer Co.,Ltd., Shanghai, 200245, China*

Received: August 22, 2025; Revised: November 19, 2025; Accepted: December 12, 2025





## Abstract

Lubrication failure of moving parts at extremely cryogenic temperatures poses a major challenge for advancements in space exploration, superconductivity, and other technologies. This study systematically investigates the tribological behavior of

* Corresponding author. E-mail: jili@licp.cas.cn

hydrogenated amorphous carbon (a-C:H) films in vacuum from -200 to 25 ℃. Notably, as temperature decreases, the friction coefficient and the wear life of the a-C:H films exhibit an abnormal increase. At -200 ℃, wear life exhibits a remarkable enhancement of at least two orders of magnitude. Introducing in situ mass spectrometry and cryogenic micro/nano indentation, the dynamic monitoring of interface damage, hydrogen passivation, and hardness evolution was conducted during the friction process. The work indicated that cryogenic temperatures significantly reduce damage of a-C:H films, leading to changes in the synergistic lubrication involving hydrogen passivation, graphitization, and transfer films, resulting in high friction and low wear. It is fundamentally attributed to cryogenic temperatures altering the interfacial activity, which is the key factor in activating the synergistic lubrication of the above mechanisms. Crucially，with a suitable interfacial activity at -75 ℃, a-C:H films can achieve an ultralow friction coefficient of ~0.015 and a wear rate of ~ $10^{-8}$ $mm^3/N \cdot m$. The work provides critical insights and establishes a foundation for deploying a-C:H films for cryogenic applications.

## Keywords

a-C:H film, cryogenic temperatures, vacuum, structural evolution, interfacial activity

## 1. Introduction

With the rapid advancement of technology, there has been a growing interest in the evolution of material structure and performance under extreme conditions. The reliable performance of materials under extreme conditions will be a key factor in future breakthroughs in cutting-edge technology. Cryogenic temperatures represent a typical

extreme environment that has attracted significant attention for superconductivity[1], hydrogen energy[2], and space exploration[3]. Tribology deals with friction and wear issues in materials under extreme conditions, and research into cryogenic tribology is becoming increasingly urgent and important. In such extreme cryogenic temperature environments, ensuring the reliable operation of moving components has become one of the key bottlenecks in the rapid development of cryogenic temperature technology.

Most lubrication materials face significant failure risks at cryogenic temperature. Conventional lubricating greases experience increased viscosity and deteriorated fluidity at cryogenic temperatures, making it difficult to perform their lubrication function[4, 5]. Solid lubricants, while offering advantages such as a wide temperature range, low evaporation rate, and corrosion resistance, also face challenges under cryogenic conditions[6, 7]. Cryogenic temperatures inhibit molecular and atomic motion, compromising bond breaking and chemical reactions during friction[8]. As a result, many solid lubricating materials do not exhibit expected tribological properties. For example, the friction coefficient of $MoS_2$-based films at cryogenic temperature is more than three times that at room temperature[9]. Additionally, in polymeric materials, molecular chains and segments freeze at ultra-low temperatures, hindering plastic deformation and stress release during friction, which leads to material fracture and increased wear[10, 11]. Some metals are susceptible to adhesive wear and seizure failure in vacuum and cryogenic conditions due to the lack of oxide film protection[12, 13]. Thus, the applicability, reliability, and longevity of existing conventional lubricant systems in deep space cryogenic temperature environments face fundamental

challenges. Moreover, while most research focuses on evaluating the tribological properties of materials at cryogenic temperatures, the research on failure mechanisms remains insufficient, making it difficult to form a unified understanding[14, 15].

The Hydrogenated diamond-like carbon (a-C:H) film is an amorphous material formed by bonding $sp^3$-C in the diamond structure and $sp^2$-C in the graphite structure, thus combining the excellent properties of diamond and graphite[16]. Its ability to achieve a durable and stable ultra-low coefficient of friction on a macro-scale makes it one of the most promising materials for space applications in terms of wear resistance and drag reduction[17, 18]. However, the tribological performances of a-C:H films in cryogenic temperature environments are still poorly researched and understood.

In this work, the tribological behavior and lubrication mechanisms of a-C:H films were investigated in vacuum from -200 to 25 ℃. We systematically investigated the formation of transfer films and graphitization processes in contact regions using Scanning Electron Microscope (SEM), High Resolution Transmission Electron Microscopy (HRTEM) and Raman mapping. In situ mass spectrometry was employed to monitor the real-time structural evolution of sliding interfaces, including hydrogen passivation and the extent of film damage. Additionally, the hardness of a-C:H films was characterized via in situ micro/nanoindentation at cryogenic temperature. This multi-modal approach reveals the underlying friction mechanisms of a-C:H films under cryogenic conditions (Fig. 1).

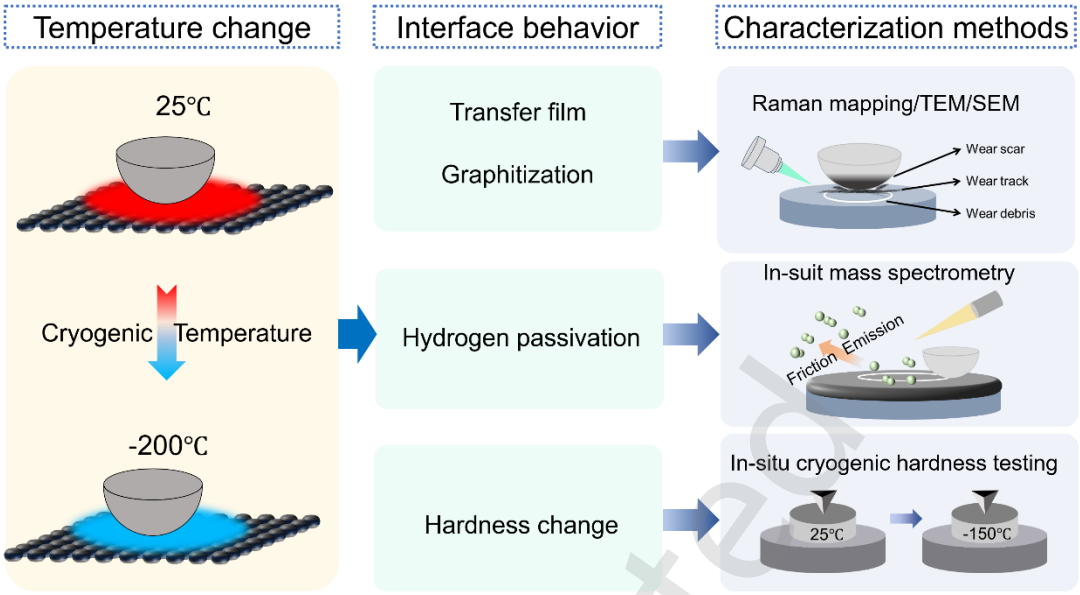


**Fig. 1.** A multi-angle characterization strategy for the tribological behavior and lubrication mechanism of a-C:H films in vacuum from -200 to 25 ℃.

## 2. Experimental procedures

### 2.1 Films deposition

The a-C:H films were deposited on polished inconel 718 alloy using reactive magnetron sputtering. The polished inconel 718 alloy was ultrasonically cleaned sequentially with anhydrous ethanol, petroleum ether, and acetone for 20 min each time to remove the oil on the surface of the substrate, and the residual liquid was blown dry with nitrogen (99.9% purity). As the base pressure of 7.0 × $10^{-3}$ Pa was achieved, a-C:H films were deposited by the following deposition parameters:(1) The surface of inconel 718 alloy was etched using $Ar^{+}$ for 40 minutes at -600 V bias pressure to remove surface oxides and contaminants and increase the roughness of the substrate. (2) The Si interfacial and Si-C gradient layers are deposited sequentially to increase the bond strength between the film and the substrate. (3) The working pressure was also kept

sustained at 0.6 Pa. (4) The ratio of argon to methane (99.9% purity, flow rate) was 13:9. (5) The sputtering deposition time was 3.5 h, and the substrate was not heated during the deposition. The thickness of the a-C:H film is ~1.5 μm, with a deposition rate of 7.6 nm/min. Calculations based on Raman spectroscopy indicate the hydrogen content in the as-deposited a-C:H films is about ~31.7 at.% (Fig. S1).

The high-hardness a-C:H film with a total thickness of 3.5 μm was deposited on inconel 718 alloy by a reactive magnetron sputtering process from acetylene ($C_2H_2$), at -650 V bias voltage. It began with the deposition of a Cr adhesion layer for 60 min (10 kW, -120 V bias voltage). Subsequently, a gradient Cr/WC interlayer was formed over 60 min by progressively ramping the Cr target power from 10 kW to 1 kW while simultaneously increasing the WC target power from 1 kW to 8 kW under an -80 V bias voltage. Finally, a WC-C:H layer was deposited by introducing acetylene. The process started with a 30-minute ramp of the $C_2H_2$ flow from 20 to 100 sccm at a bias voltage of -50 V. Then, with the WC target turned off, the conditions were stabilized at a $C_2H_2$ flow of 50 sccm and a high bias voltage of -650 V for 3 hours to complete the formation.

**2.2 Tribological Test**

In order to evaluate the tribological properties of a-C:H thin films in cryogenic vacuum environments, a self-developed ball-on-disc cryogenic vacuum tribometer (CDW-400, Huayu Aerospace Technology Application Company Limited, Lanzhou) was used for testing. The cryogenic vacuum tribometer comprises refrigeration, vacuum, and friction. Two independent servo motors control rotational speed and normal load during the friction process. The normal loading force sensor boasts an

accuracy of 0.5% F.S., and the friction force sensor achieves 0.05% F.S. accuracy. With a sampling frequency of 50 Hz, the coefficient of friction μ is calculated as the ratio of the friction force F to the applied load N. Refrigeration is achieved through the adiabatic process within the Gifford-McMahon (GM) refrigerator, which expands and cools the gas to generate the required refrigeration capacity. The a-C:H film is cooled through heat conduction from the cold head of the GM refrigerator. In order to reduce heat loss, an indium sheet was placed between the a-C:H film and the cold head.

The test temperatures were 25 ℃, -50 ℃, -100 ℃, -150 ℃ and -200 ℃. The a-C:H film deposited on inconel 718 alloy was fixed on a refrigeration platform, and the film was cooled by heat conduction. In order to reduce heat loss, an indium sheet was placed between the film and the refrigeration table. The counterpart ball is a commercially available GCr15 ball (Φ = 6 mm, Ra ~ 18 nm), and a servo motor controls the load during the experiment. The test load was 5 N, the rotation radius was 5 mm, the sliding speed was 6.28 cm/s. The ultimate vacuum pressure within the tribometer chamber can reach ~ $2 \times 10^{-3}$ Pa at room temperature. However, the vacuum pressure decreases further due to the effect of the cold trap at cryogenic temperatures. To minimize the impact of vacuum pressure on the experiment, the chamber was first evacuated to its ultimate vacuum ($2 \times 10^{-3}$ Pa) at room temperature prior to sample cooling. Stable pressure ranges of 1.8 to $2.0 \times 10^{-3}$ Pa at 25 °C and 6.0 to $8.0 \times 10^{-5}$ Pa at -200 °C were maintained throughout friction testing. In addition, all the friction test experiments were repeated 3 times at least. The wear rate is calculated as V/(F•L), where V is the total wear volume, F is the applied load, L is the sliding length.

### 2.3 In-situ Cryogenic Hardness Test

The cryogenic hardness of a-C:H films was examined in real-time using a cryogenic micro- and nanoindentation tester developed by Jilin University. A load of 100 mN was applied, utilizing a Berkovich diamond indenter ($\alpha = 65.3° \pm 0.3°$). To mitigate measurement bias due to the indenter's temperature, both the indenter and film were cooled with liquid nitrogen. Before formal testing, the temperature of the indenter and film was maintained as consistently as possible through direct contact. The morphology of the indent at varying temperatures was observed using a field emission SEM.

### 2.4 Film Characterization

The surface morphology of the contact area was obtained using an optical microscope (Olympus STM3). Raman spectral mapping of $102 \times 102$ μm$^2$ (with a step of 6 μm) at the wear track of the a-C:H films was conducted at room temperature using a Laser Micro-Raman Spectrometer (Renishaw inVia, UK). The $Ar^+$ exciter wavelength was 532 nm, and the laser beam was focused using a ×20 objective lens with a scanning wave number range of 100-3200 cm$^{-1}$ and a scanning time of 10 s/point. The wear debris produced by friction at different temperatures were prepared on a copper mesh (230 mesh), and the wear debris morphology was observed using a transmission electron microscope (FEI Tecnai 20, USA). The hardness of the high-hardness carbon films were evaluated by nanoindentation measurements (NHT$^2$, CSM, Switzerland) using a Berkovich diamond indenter. A maximum load of 10 mN was applied during testing, with the penetration depth carefully controlled to ~ 1/10 of the total film thickness to

minimize substrate effects.

### 2.5 Mass spectrometer Test

The Quadrupole Mass Spectrometer (Prismapro QMG250, Pfeiffer Vacuum GmbH) is connected to the cryogenic vacuum tribometer via a flange. Before starting the friction test, turn on the mass spectrometer and select the fast scan mode, which has a single scan duration of 9.72 s and a relative mass range of 1-50. Engage the electron multiplier to improve the capture of ion current signals. The mass spectrometer was operated continuously for 5 minutes to allow stabilization of major molecular intensity (such as $H_2O$ and $N_2$) within the chamber, thereby minimizing potential experimental interference prior to initiating friction testing. During the friction stage, changes in the content of various molecular and fragment ions are recorded in the chamber. Once the friction test is finished, turn off the mass spectrometer immediately.

## 3. Results and Discussions

### 3.1. Tribological behavior of a-C:H films in vacuum from -200 to 25 ℃

Fig. 2 shows the tribological behavior of a-C:H films under cryogenic vacuum conditions. We can see that the friction coefficient is lower than 0.01 at 25 ℃, but the wear life can only be maintained for 700 s (Fig. 2(a)). As the temperature decreases, the interfacial activity between the GCr15 balls and the a-C:H film is weakened, and the wear life of the a-C:H film shows a significant increase. At -50 ℃, the wear life of the film increased from 700 s to 2200 s while maintaining a low friction coefficient. When the temperature was lowered again to -100 ℃, the friction coefficient of the film showed a tendency to increase, and the film did not fail after one hour of rubbing. At -

150 ℃ and -200 ℃, the films had a high friction coefficient of 0.2, but their wear rate showed a trend opposite to the coefficient of friction. At -200 ℃, the film had the lowest wear rate of $5.82\times10^{-8}$ $mm^3/N\bullet m$ (Fig. 2(b)). The depth of the wear tracks of the a-C:H film after friction for 1 hour at -100 ℃, -150 ℃, and -200 ℃ was observed using a three-dimensional profilometer. The wear tracks of the a-C:H film are very shallow, with an overall abrasion depth of no more than 50 nm. It indicates that although cryogenic temperature leads to a high friction coefficient of a-C:H films, it also significantly enhances the wear life. Compared with other cryogenic lubricants reported in the literature, such as $MoS_2$, PTFE, and Cu, a-C:H film exhibits the lowest wear rates (Fig. S2), demonstrating its significant application potential under cryogenic conditions.



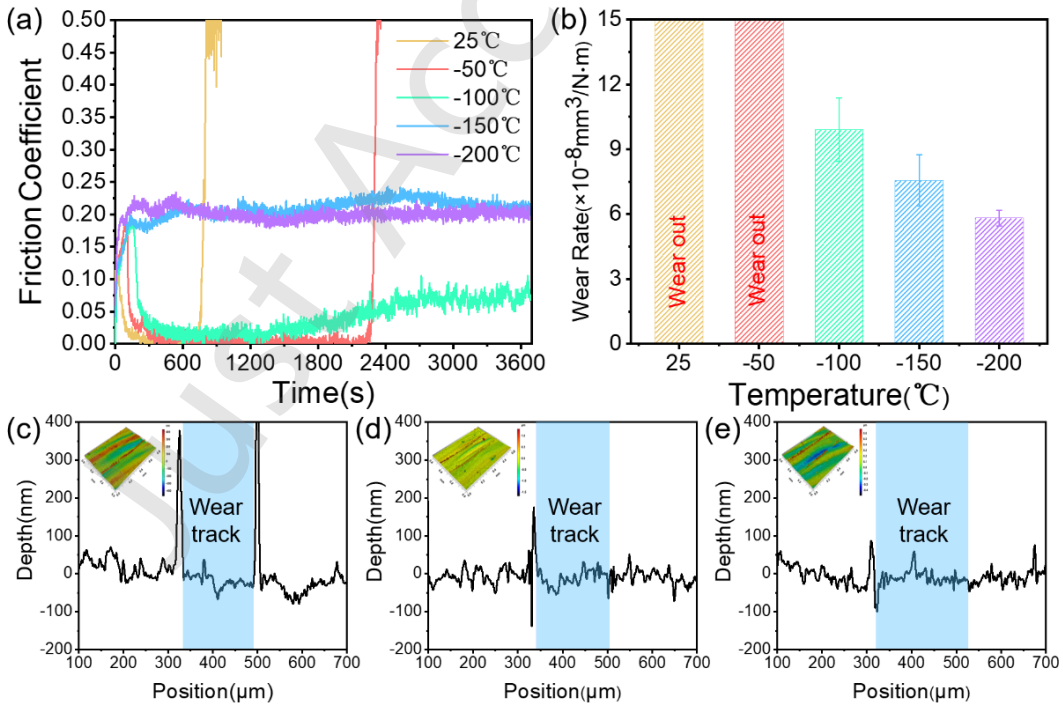


**Fig. 2.** Tribological behavior of a-C:H films under cryogenic vacuum conditions. (a) friction coefficient, (b) wear rate, (c) wear tracks at -100 ℃, (d) wear tracks at -150 ℃, (e) wear tracks at -200 ℃.

### 3.2. Structural evolution of transfer film from -200 to 25 ℃

The reduction of the friction coefficient of the carbon film is often accompanied by the formation of the transfer film on the surface of the counterpart ball, which changes the strength of the interfacial activity between the friction pair[19, 20]. Fig. 3(a)-(e) show the optical morphology photographs of GCr15 ball wear scars at different temperatures before film failure. At 25 ℃, obvious transfer films can be seen observed on the GCr15 ball, and some of these transfer films are thick and dense (Fig. 3(a)), which indicated indicating that strong interfacial adhesion was generated during the friction process. At -50 ℃, the wear scars began to become larger, and the transfer film was colored, but there was no thicker transfer film, which indicated that the transfer capacity of carbon to the surface of GCr15 ball was gradually weakened. With the further reduction of temperature, the wear scar gradually increases in size, while the transfer film decreases and appears only at the edge of the wear scars. By comparing the optical morphology of the wear tracks at five temperatures (Fig. 3(f)-(i)), it can be observed that in the stabilization phase before film lubrication fails, the wear tracks become progressively wider and more obvious as the temperature decreases. The results indicate that the transfer of a-C:H films to the GCr15 ball is inhibited at cryogenic temperatures. It is generally accepted that the tribological behavior of a-C:H films in a vacuum is related to the interaction between the sliding interfaces. The stronger the activity between the sliding interfaces, the easier the carbon transfer to the counterpart surfaces occurs, which reduces the friction coefficient. However, it also leads to an increase in film damage and a shorter lifetime. At cryogenic temperatures, the formation

of transfer films is inhibited, which increases the coefficient of friction and reduces the wear of a-C:H films.

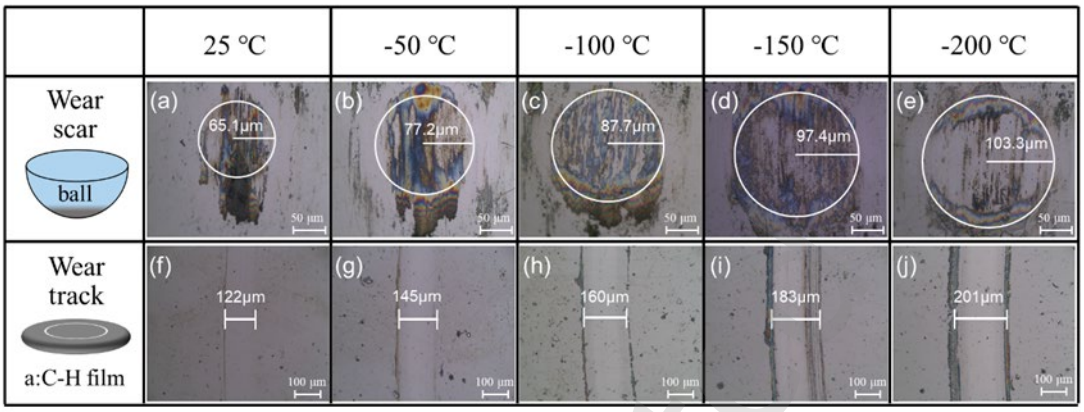


**Fig. 3.** Optical micrographs of wear scars and wear tracks at different temperatures before friction failure: (a)(f) 25 ℃; (b)(g) -50 ℃; (c)(h) -100 ℃; (d)(i) -150 ℃; (e)(j) -200 ℃. (The wear tracks at 25 ℃ and -50 ℃ were obtained after 5 minutes of friction, while those at -100 ℃, -150 ℃ and -200 ℃ were observed after 1 hour of friction.)

The morphology of the wear scar was further analyzed using SEM, as shown in Fig. 4. The results show that the carbon on the counterpart ball is more concentrated in the center region of the wear scar at room temperature. As the temperature decreases, the carbon on the counterpart balls gradually decreases and transfers toward the edge of the wear scar. Scanning the carbon distribution of the wear scars by Energy-dispersive X-ray spectroscopy(EDS) shows that the carbon transferred on the counterpart ball is thicker at room temperature. At -200 ℃, there is almost no carbon in the center area of the wear scar, with only a little carbon existing at the edge, and the result is consistent with that of the light microscope. It indicates that with the decrease in temperature, the transfer of a-C:H film to the counterpart ball during the friction process is suppressed, and the friction interface changes from the carbon-to-

carbon interaction at room temperature to the GCr15 ball-to-carbon film interaction at cryogenic temperature.

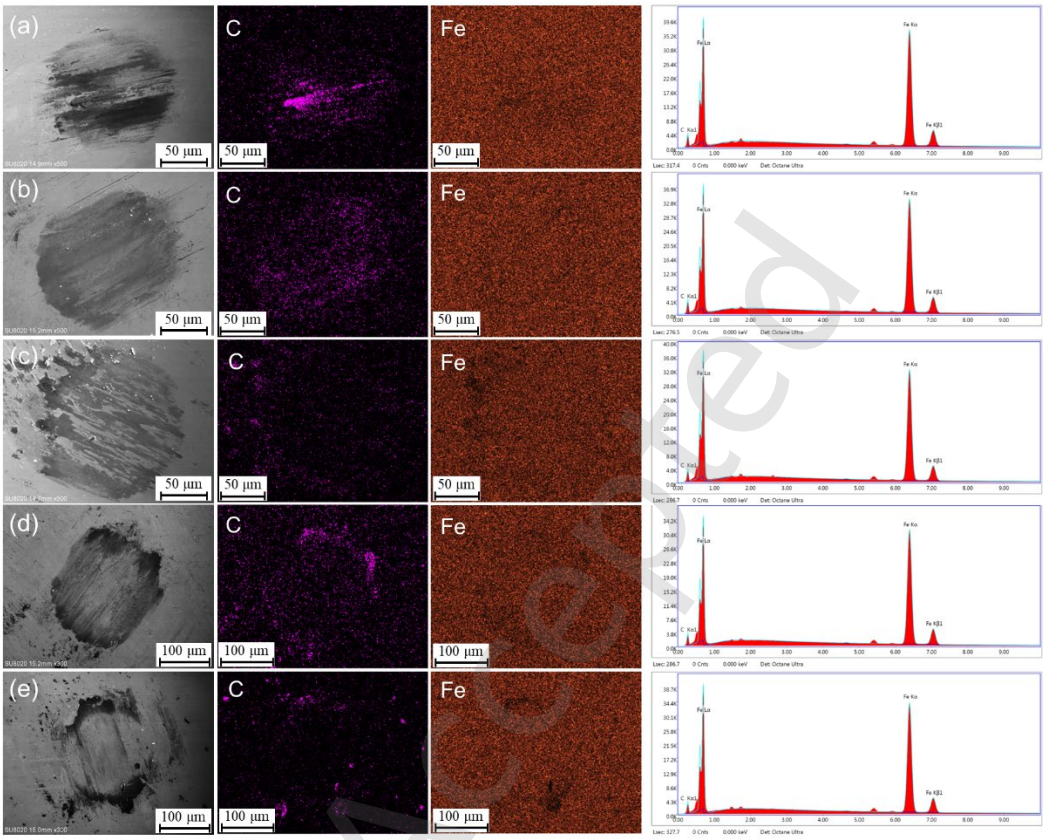


**Fig. 4.** SEM images and EDS elemental distribution maps of wear scars at different temperatures before friction failure: (a)(f) 25 ℃; (b)(g) -50 ℃; (c) (h) -100 ℃; (d)(i) -150 ℃; (e)(j) -200 ℃.

It is well known that the evolution of the interface structure during the run-in period is often dramatic, and at this stage, the counterpart rapidly damages the a-C:H films. Fig. 2(a) showed that a running-in period existed before achieving stable friction conditions. With decreasing temperature, the duration of the running-in period initially increased before decreasing. It occurred because reduced interfacial activity at cryogenic temperatures slowed carbon transfer to the GCr15 ball, thereby prolonging the time required to form a stable transfer film and lubricating interface. Transfer film

formation becomes significantly more challenging at -150 ℃ and -200 ℃. Sliding primarily occurs between the GCr15 and the a-C:H films rather than between the C/C surfaces, necessitating a shorter running-in period. It led to an increase in the friction coefficient. Does forming a dense transfer film on the surface of GCr15 balls before friction, which would reduce the running-in period and the friction coefficient?

To further investigate the role of the transfer film in reducing friction, the GCr15 ball was allowed to rub against the a-C:H film beforehand and formed a dense transfer film. The GCr15 ball with the transfer film was then rubbed against a-C:H film at -200 ℃ (Fig. S3(a) and S3(b)). When comparing the friction coefficients of the a-C:H films in two scenarios, it's observed that the friction coefficient of the GCr15/a-C:H without the transfer film rapidly increased to 0.22 during the initial friction stage and then stabilized around 0.2. In contrast, the GCr15/a-C:H with the transfer film exhibited a lower friction coefficient during the running-in period. However, after a running-in period of 300 s, the friction coefficient increased to 0.2, indicating that the transfer film reduced friction. Nevertheless, the structural changes and interactions occurring at the interface were intense during this period, making it difficult for the transfer film to remain stable on the GCr15 surface. As a result, it was rapidly destroyed and failed to provide a lasting effect. Concurrently, the cryogenic temperature inhibited the replenishment of the transfer film, leading to consistent friction coefficients during the stable phase. It is evident that while the transfer film formed during the running-in period serves to reduce friction, its effectiveness relies upon a stable sliding interface and the continuous replenishment of carbon.

### 3.3. Structural evolution of wear debris from -200 to 25 ℃

The structural evolution of the friction interface plays a pivotal role in determining the tribological properties of a-C:H films in vacuum. The wear debris structure of the friction interface at different temperatures when the film did not fail was analyzed using transmission electron microscopy (Fig. 5). The findings reveal that the wear debris structure at the contact interface primarily exhibits an amorphous structure at room temperature (Fig. 5(a)). A structurally ordered slip layer is present on the surface, suggesting that frictional shear triggers an ordered transformation of the interface's atomic structure. This transformation is crucial for maintaining the low friction coefficient of the a-C:H films at room temperature in vacuum. At -50 ℃, a minor curled structure emerged in the wear debris, which was imperfect. There appeared to be some bent or folded nanotubes at -100 ℃.As the temperature decreased, more completely curled structures were observed in the wear debris at -200 ℃ However, these structures did not lead to a reduced coefficient of friction. It can be attributed to the fact that cryogenic temperatures make it more difficult for the transfer film to migrate toward the counterpart ball. The amorphous carbon produced at the interface during friction curls under force, forming this imperfect curled structure. The lower the temperature, the higher the coefficient of friction, and the more curled structures are formed. It indicates that in the case of less transfer film, the high friction force drives amorphous carbon to transform into curled structured carbon.

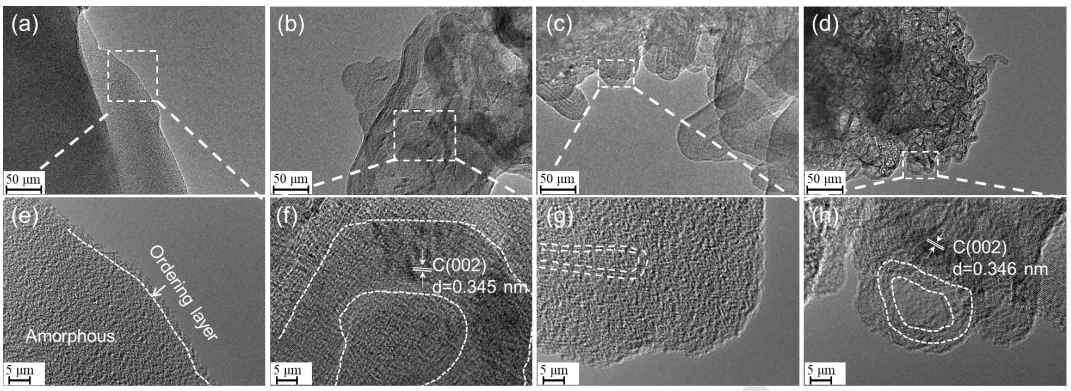


**Fig. 5.** HRTEM images of wear debris generated at the friction interface under different temperatures: (a)(e) 25 ℃; (b)(f) -50 ℃; (c)(g) -100 ℃; (d)(h) -200 ℃.

### 3.4. Structural evolution of wear tacks from -200 to 25℃

The atomic bonding of the a-C:H film wear tracks was examined by decomposing the Raman peaks into D and G peaks using Gaussian fitting. The D peak, located at 1360 $cm^{-1}$, and the G peak, at 1555 $cm^{-1}$, correspond to the $sp^2$ breathing vibration and stretching vibration, respectively[21]. The area ratios of the D and G peaks, represented by $I_D/I_G$, suggest that larger $I_D/I_G$ ratios indicate a larger $sp^2$ cluster enhanced bonding order within the amorphous carbon matrix. The $sp^2$ -C content can be inferred by comparing the $I_D/I_G$ values of wear tracks at different temperatures, thus studying the degree of graphitization of the films after friction. Fig. 6(a) shows the Raman mapping of the pristine surface of the prepared amorphous carbon hydrogen (a-C:H) films, which have $I_D/I_G$ values ranging from 1.0 to 1.3. Subsequently, the Raman mappings of the wear tracks at five temperatures were compared under steady-state friction conditions. The $I_D/I_G$ values of the wear tracks at temperatures of 25 ℃ and -50 ℃ were predominantly above 1.7 (Fig. 6(b), (c)), indicating a significant increase in the degree of graphitization compared to the pristine film surface. When the temperature reached

-100 ℃ and -150 ℃, the $I_D/I_G$ values of the wear tracks significantly decreased, mostly around 1.5 (Fig. 6(d)). As the temperature continued to decrease, it was observed that the $I_D/I_G$ values in the wear mark areas at -200 ℃ were even smaller, suggesting that graphitization is more challenging to occur at cryogenic temperatures.

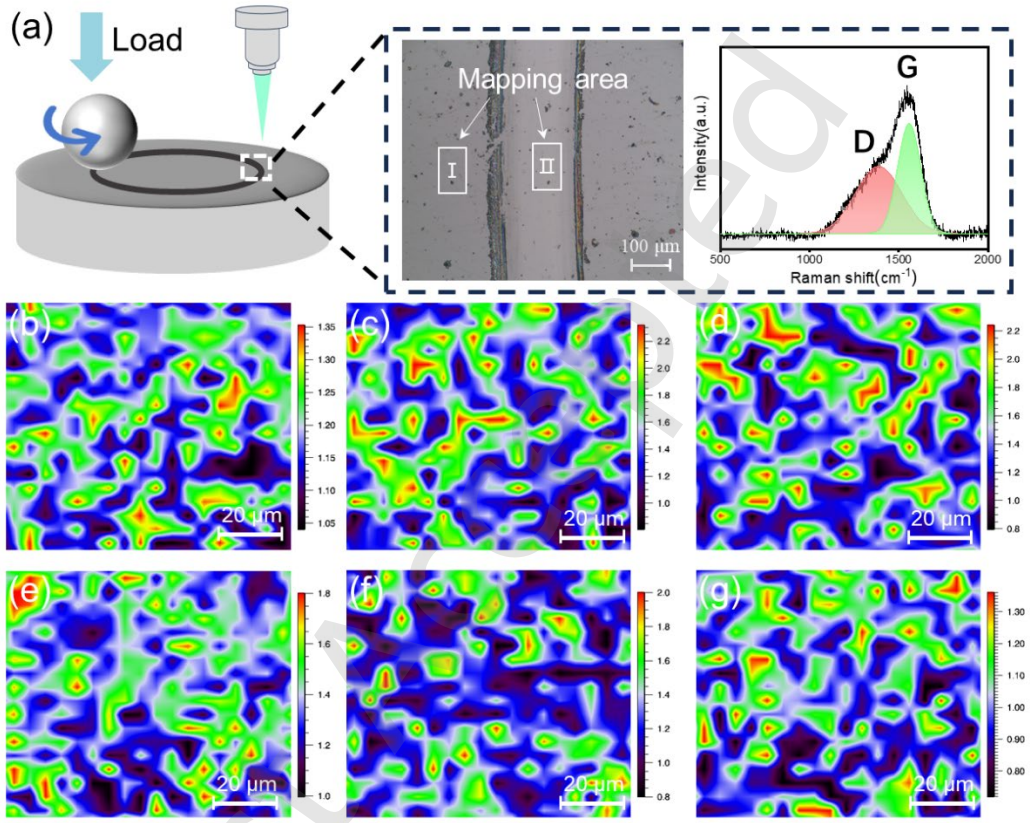


**Fig. 6.** (a) Raman spectra of the original surface and the abraded area at different temperatures; (b) Raman mapping of the original a-C:H film surface and (c) wear tracks at 25 ℃; (d) -50 ℃; (e) -100 ℃; (f) -150 ℃; and (g) -200 ℃.( The wear tracks at 25 ℃ and -50 ℃ were obtained after 5 minutes of friction, while those at -100 ℃, -150 ℃ and -200 ℃ were observed after 1 hour of friction.)

The degree of graphitization of thin films not only depends on the friction force, but the ambient temperature of the sample also has an effect. High friction forces result in increased local shear stresses and frictional heat at the interface, potentially causing

the substable $sp^3$ phase to relax into the $sp^2$ phase[22]. The flash temperature rise at the contact interfaces can be estimated using the following equation[23, 24]:

$$\Delta T = \frac{\mu F_n v}{4a\left(K_{a-C:H}+K_{GCr15}\right)} \quad (1)$$

Where $\Delta T$ is the flash temperature rise at the contact bump, μ is the friction coefficient, and Fn is the applied normal load. In this work, the load Fn is 5 N, the sliding speed ν is 0.0628 m/s, $a$ is the actual contact radius (it is primarily estimated based on the size of the wear scar), and $K_{a\text{-}C:H}$ and $K_{GCr15}$ are the thermal conductivity of the a-C:H film and the GCr15 ball, respectively. From equation (1), the larger the friction coefficient, the higher the temperature rise at the contact interface when the applied normal load and velocity are certain. Graphite is thermodynamically more stable than a-C:H film, so the increase in $sp^2$-C during the friction process is predictable. As the ambient temperature decreases, the heat generated during friction transfers more to the cryogenic region, which does not provide enough energy for graphitizing the friction interface. Research indicates that the transition from a $sp^3$-rich diamond-like phase to a $sp^2$-dominated graphite-like phase primarily depends on stress relaxation[25]. The stress relaxation is achieved by migration or transfer of atoms in the interfacial region, which can induce the transformation of the $sp^3$-C to the $sp^2$-C at lower temperatures than the annealing temperature[23]. At high friction forces, the strain energy at the friction interface increases, allowing it to accomplish the deformation required for the film's transition to graphite following the release of hydrogen atoms. However, cryogenic temperatures limit the migration of atoms and the release of hydrogen from the friction interface, so the onset of graphitization under these

conditions is difficult, resulting in an increase in the friction coefficient of the a-C:H films.

### 3.5 Evolution of chemical products at friction interfaces from -200 to 25 ℃

The friction behavior between contact interfaces often leads to the generation of several products, and dynamically monitoring these provides effective insight into the evolution of friction. Fig. 7(a) shows a schematic diagram of the online detection device for debris ions. Fig. 7(b)-(c) demonstrates the changes in the content of fragment ions for two main different mass-to-charge ratios (m/z) of a-C:H thin films during friction at cryogenic temperatures. With the onset of friction, the contents of two fragment ions show an increasing trend, indicating the strong generation and frictional release of hydrocarbon molecules corresponding to the contact interface during friction.

Molecules with m/z =2 can be identified as hydrogen molecules ($H_2$). The escape rate of hydrogen molecules from the film is markedly higher at room temperature compared to cryogenic temperatures. It implies that counterpart balls inflict more damage on a-C:H films at room temperature than at lower temperatures. A comparison with Fig. 2(a) reveals that a low friction coefficient correlates with a high hydrogen escape rate, suggesting that substantial hydrogen release can reduce the friction coefficient. When the friction coefficient suddenly increases, the escape rate of hydrogen molecules also rises. Molecules with a m/z =15 can be identified as $CH_3$• ions, originating from hydrocarbon molecules formed by destroying a-C:H films. The production rate of $CH_3$• ions is highest at room temperature and lowest at -200 ℃, indicating greater disruption of the a-C:H films at room temperatures, resulting in

numerous hydrocarbon molecule. At cryogenic temperatures, the reduction in damage to carbon films by the counterpart results in a longer lifespan for a-C:H films. During friction failure, there is also a significant increase in the content of $CH_3$• ions. The changes in the content of $H_2$ and $CH_3$• ions directly correlate with the degree of damage to the a-C:H film and hydrogen passivation during the friction process from -200 to 25 ℃.

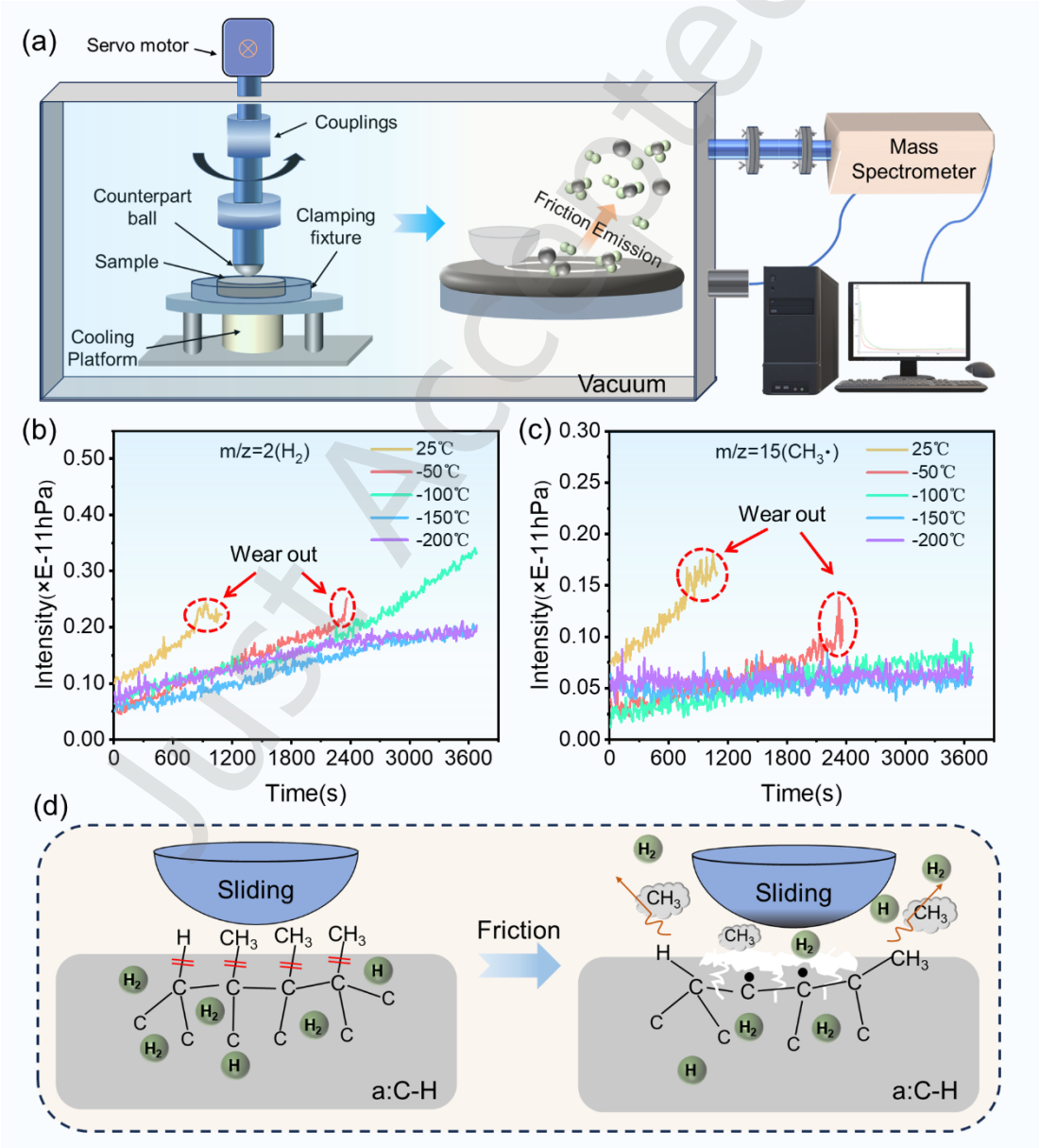


**Fig. 7.** (a) Schematic diagram of an in-suit detection device for friction fragments.

Variation of two main fragments contents during friction at different temperatures: (b) $H_2$ (m/z=2), (c) $CH_3$• (m/z=15). (d) Schematic diagram of product generation at the friction interface

Previous studies have demonstrated that hydrogen plays an important role in the friction of carbon films[26-28]. The chemical bonds in a-C:H films in a vacuum are broken by repeated friction processes, and the wear surface exposes a large number of dangling bonds, which generate strong chemical activity on the friction surface, leading to a high coefficient of friction of the a-C:H films, and thus to a rapid failure[29]. From Fig. 7(b) and (c), it can be seen that although the a-C:H film has the lowest friction coefficient at 25 °C, the escape rate of hydrogen and the fragmentation molecule $CH_3$• is the fastest. At room temperature, the GCr15 ball induces significant degradation of the a-C:H film, causing rapid structural deterioration. The enhanced molecular mobility at this temperature also leads to a sharp increase in fragment ion concentration. Concurrently, substantial hydrogen desorption increases the probability of dangling bond passivation, thereby contributing to a low friction coefficient. However, these two competing mechanisms result in the characteristic coexistence of low friction coefficients and severe wear observed in a-C:H films. As the temperature decreases, the damage caused by the GCr15 ball to the a-C:H film is reduced, and molecular motion becomes further restricted. Consequently, fewer fragment ions escape from the damaged interface.

Fig. 7(d) shows a schematic representation of the generation of hydrogen and methane ions during the friction process. Initially, numerous hydrocarbon groups

(CxHy) are present on the film's surface and are connected by chemical bonds. As the sliding friction occurs, the GCr15 ball experiences intense collisions and adhesion with the a-C:H films. This interaction causes the bonds of the surface hydrocarbon groups at the contact interface to break, leading to their emission from the surface. The newly formed unsaturated carbon-hydrogen bonds exhibit high chemical reactivity and can strongly interact with the carbon transfer film and GCr15 ball, which increases wear.

At room temperature, the strong chemical reactivity between GCr15 balls and a-C:H films causes significant damage to the a-C:H film. Under friction and heat, hydrogen within the a-C:H films rapidly escapes into the environment, which in turn passivates the dangling bonds at the interface. In contrast, at cryogenic temperatures, the interaction between GCr15 balls and a-C:H films is reduced, resulting in minimal carbon transfer to the surface of the GCr15 balls, indicating less damage to the a-C:H films. The lower temperature and reduced pathways also affect the hydrogen within the film, leading to less hydrogen escape.

**3.6 Effect of hardness for the tribological behavior from -200 to 25 ℃**

In order to investigate whether the mechanical properties of a-C:H films are altered at cryogenic temperatures, thus affecting its tribological behavior. We have characterized the hardness of a-C:H films using an in-suit cryogenic micro- and nanoindentation instrument. Fig. 8 illustrates the high-resolution SEM morphology of indentations on a-C:H films at various temperatures. In Fig. 8(a), the indentation morphology at 25 °C is clearly visible, with noticeable cracks in the center of the indentation, which has an area of 28.56 μm². As the temperature decreases, the

indentation area significantly reduces. At -150 °C, the indentation area is only 16.62 μm². Generally, an increase in a material's hardness can lead to fewer contact interfaces during friction, resulting in a smaller interaction area at the contact points, thereby enhancing wear resistance.

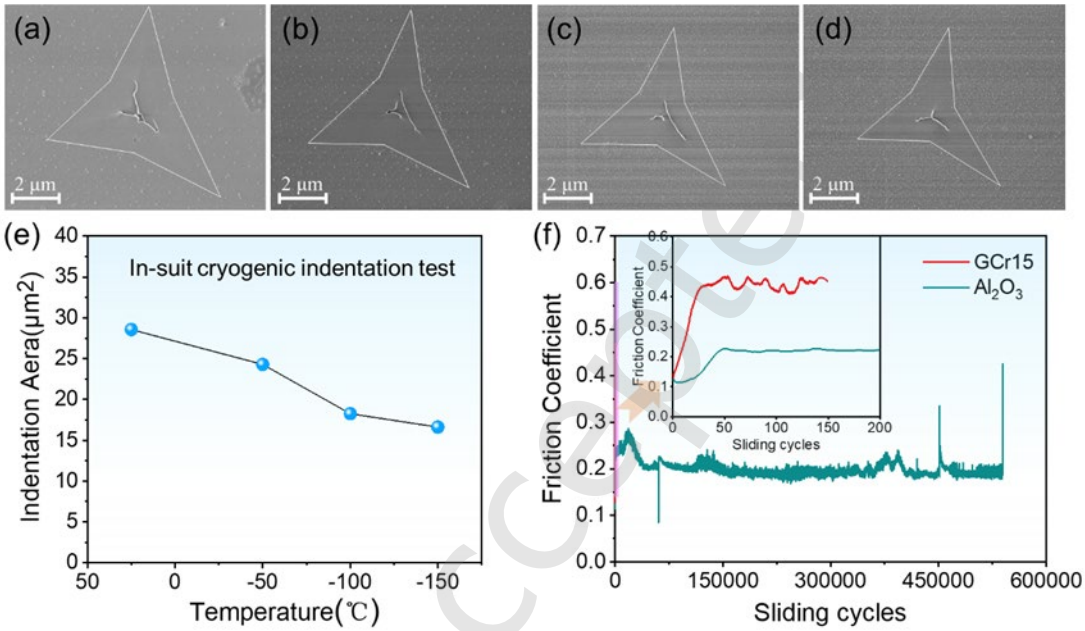


**Fig. 8.** SEM images of in situ cryogenic indentation morphology of a-C:H films: (a) 25 ℃; (b) -50 ℃; (c) -100 ℃; (d) -150 ℃. (e) In situ cryogenic indentation area at cryogenic temperature. (f) Friction coefficient of high-hardness a-C:H films with GCr15 ball and $Al_2O_3$ ball in vacuum at 25 ℃.

It raises the question of whether merely increasing the hardness of the a-C:H films can extend its lifetime in a vacuum. To further test this hypothesis, we selected a a-C:H film with higher hardness to conduct friction tests with the GCr15 ball (Fig. S4). The wear life of the high-hardness a-C:H films with GCr15 ball in vacuum at room temperature remains significantly short, considerably lower than that of the original low-hardness a-C:H film (Fig. 8(f)). Therefore, simply increasing hardness does not

fundamentally change the wear life of hydrogen-containing carbon films in vacuum. There are other reasons that play a dominant role.

The tribological properties of a-C:H films are closely related to the environment. Although lubrication theories such as hydrogen passivation, graphitization, and transfer films have been proposed, a key challenge is that the presence of complex mechanochemical interactions and dynamic structural evolution during the friction process leads to limitations of these theories[30-32]. Friction originates from the interaction between sliding interfaces. The fundamental principle underlying the three aforementioned lubrication mechanisms stems from variations in the interfacial interaction strength. At cryogenic temperatures, however, the restricted molecular and atomic motion within the constituent materials alters the interfacial activity. This temperature-dependent variation in interfacial activity provides a robust explanation for the different lubrication mechanisms observed. To validate this hypothesis experimentally, we conducted friction tests using $Al_2O_3$ balls and higher hardness a-C:H films.

Compared to the GCr15 balls, the interfacial activity between the $Al_2O_3$ balls and the a-C:H film is weak. The experimental results demonstrate that the wear life of the film can reach $5.4 \times 10^5$ cycles under the experimental conditions of a 5 N load and a line speed of 26.17 cm/s (Fig. 8(f)). It suggests that the activity between the friction interfaces is the primary factor in achieving a long life for a-C:H films in vacuum. During friction, it is more challenging for the weakly chemically active counterpart balls to cause significant damage to the carbon film, resulting in less wear debris on the

$Al_2O_3$ balls. Although the weakly chemically active counterpart balls can significantly extend the vacuum lifetime of the a-C:H films, the friction coefficient is higher due to the difficulty of forming a dense and ordered shear layer at the friction interface. It is consistent with the change in tribological behavior of GCr15/a-C:H film at cryogenic temperatures. While the counterpart material with weak interactions with the a-C:H films can extend wear life in a vacuum, the friction coefficient cannot be reduced unless an effective lubricating layer is established at the contact interface.

### 3.7 Tribological behavior and interfacial structure of a-C:H film at -75 ℃

If the strength of interfacial activity is a dominant factor in the vacuum tribological properties of a-C:H films, then adjusting the strength can modulate various lubrication mechanisms, leading to low friction coefficient and wear of a-C:H films in a vacuum environment. Fig. 2(a) indicates that the friction coefficient increases considerably between -50 °C and -100 °C, suggesting there is an optimal temperature within this range that achieves low friction for a-C:H films. We selected -75 °C as the test temperature. At this temperature, the friction coefficient of GCr15/a-C:H film remains around 0.015 during the stabilization phase, and the wear tracks are nearly indistinguishable (Fig. 9). Analysis of the surface morphology of the GCr15 ball shows a significant amount of transfer films, indicating that at -75 °C, there is still a strong interaction between GCr15 ball and the a-C:H films. Although this interaction leads to carbon transfer to GCr15 ball, the damage to a-C:H films caused by GCr15 is greatly reduced compared to room temperature. Moreover, interfacial graphitization and hydrogen passivation remain effective and are not significantly inhibited. Consequently,

low friction and a long lifespan for a-C:H films are achieved in a vacuum environment.

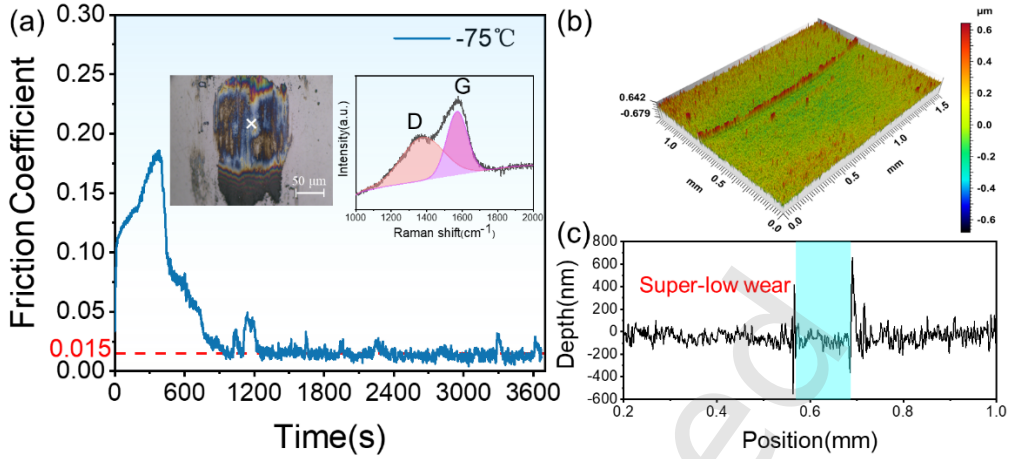


**Fig. 9.** (a) Friction coefficient maps, photomicrographs, and structural analyses of transfer films of a-C:H films at -75 ℃; (b) Three-dimensional contour and (c) depth maps of wear tracks.

To more vividly reveal the underlying mechanisms, transmission electron microscopy was employed to characterize the interfacial structures of the wear scar (Fig. 10). Apparently, a transfer layer was formed on the sliding surfaces, which protected the interfaces from direct contact and wear. The transfer layer consists of two main components: the upper layer, which is primarily composed of an amorphous carbon structure containing small amounts of iron, and the lower layer, a tribochemical layer approximately 3 nm thick that is mainly made up of $Fe_3C$ and carbon. Notably, a significant number of (002)-oriented graphite sheets are present between these two layers, aligned parallel to the direction of friction. These graphite sheets, which exhibit low interlayer shear, greatly reduce resistance during the friction process. During friction, a strong interaction occurs between the carbon and the steel balls, leading to the formation of $Fe_3C$. This frictional chemical layer of $Fe_3C$ prevents direct contact

between the steel balls and the carbon film, effectively extending the wear life of the a-C:H films. Additionally, the activity of the carbon dangling bonds is partially inhibited at -75 ℃, which weakens the strong σ interaction of C-C at the interfaces. However, hydrogen can still passivate friction-generated dangling bonds at this temperature. The combined effects of these lubrication mechanisms allow the a-C:H films to maintain a low friction coefficient and reduce wear.

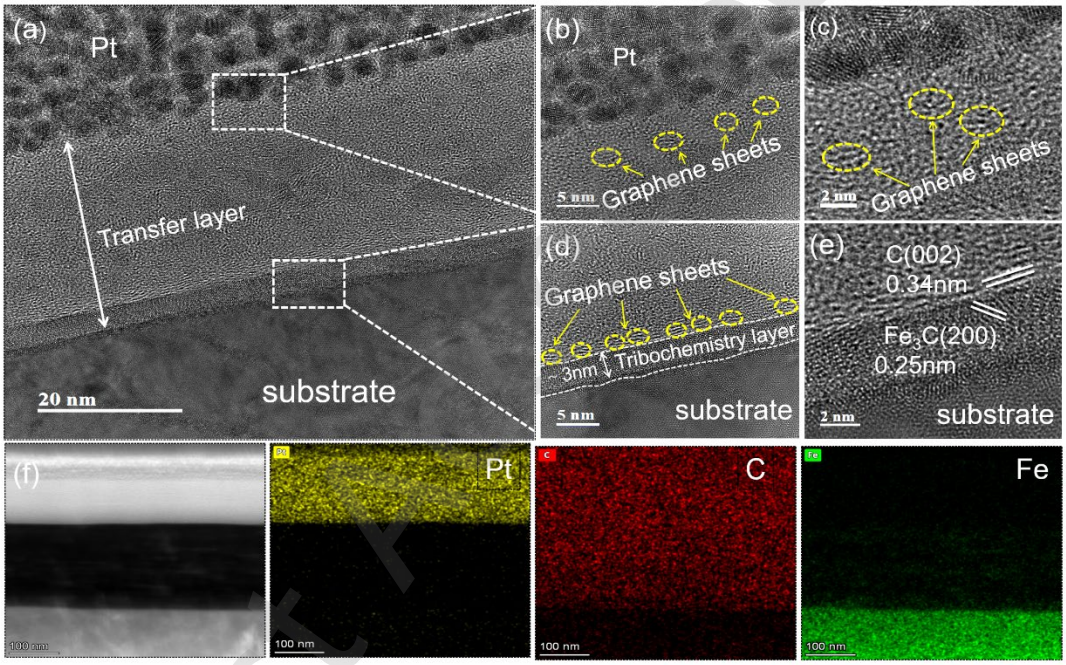


**Fig. 10.** Characterizations of the wear scar on the steel ball surface. (a) HRTEM image exhibits the cross-sectional morphology of the steel ball contact surface with a thick transfer layer formed in the wear scar, in which the HRTEM images (b-e) clarify the local structures of the transfer layer, and (f) EDS element mapping in the transfer layer.

### 3.8 Friction and wear mechanism of a-C:H film from -200 to 25 ℃

Interfacial activity refers to the dynamic ability of sliding surfaces to facilitate atomic-scale restructuring, energy dissipation, and chemical interactions, influenced by factors such as temperature, mechanical stress, and environmental conditions. It reflects

the dynamic variation in the strength of interactions between two contacting interfaces. At cryogenic temperature, interfacial activity influences the tribological behavior of a-C:H films by altering the interaction strength between GCr15 and the a-C:H films, and regulating the processes of hydrogen passivation, graphitization, and transfer film at the lubricated interface.

Fig. 11 illustrates a schematic diagram of the vacuum lubrication mechanism of a-C:H films as a function of temperature. The interfacial activity is the key to regulating the trade-off between friction and wear at cryogenic temperatures. Specifically, the strength of the interfacial interaction between the counterpart and the a-C:H films directly influences the wear resistance. Meanwhile, the friction coefficient is governed by three lubricant mechanisms: hydrogen passivation, transfer film formation, and graphitization at the sliding interface.

At room temperature, significant interfacial interactions occur between the a-C:H film and the GCr15 ball, leading to substantial carbon transfer to the surface of the GCr15 ball. The transfer changes the friction interface from GCr15/carbon to a carbon/carbon interface with lower shear strength. However, the extensive carbon transfer can severely damage the a-C:H films while simultaneously producing much hydrogen, which helps to passivate the carbon dangling bonds at the friction interface. When force and frictional heat are applied, the high degree of graphitization at the wear marks can help reduce the friction coefficient to some extent. However, it is important to note that strong interactions at room temperature can lead to poor stability of the lubricating layer formed at the contact interface. To maintain this layer effectively, a

sufficient amount of carbon is necessary. Consequently, while the a-C:H film displays a low coefficient of friction, its lifespan is limited.

As the temperature decreases, the friction coefficient and wear life of the a-C:H film show a significant increase. This unusually high friction coefficient and low wear rate are attributed to changes in the contact interface activity at cryogenic temperatures. At cryogenic temperatures, the activity at the contact interface gradually diminishes, leading to a weaker interaction between the GCr15 ball and the a-C:H film. Consequently, the damage caused by the GCr15 ball during the friction process is reduced, resulting in an extended wear life for the film. Simultaneously, this weakened interface activity makes it difficult to form a transfer film, hydrogen passivation, and graphitization, which prevents the establishment of an effective low-shear lubrication interface. As a result, a high friction coefficient is observed. Additionally, while the hardness of the a-C:H film increases at cryogenic temperatures, the contact area during friction decreases, further enhancing the film's wear resistance.

To quantitatively characterize the temperature-dependent decay of interfacial activity and its dominant influence on cryogenic friction behavior, we employed the $CH_3$• ion generated by C-H bond cleavage during friction as a chemical probe. We determined its escape rate k (Table S1) and calculated the apparent activation energy *E*a using the Arrhenius equation. Results indicate that the escape rate of $CH_3$· ions decreases with decreasing temperature, suggesting elevated energy barriers for atomic rearrangement and bond formation reactions at the interface (Fig. S5). It leads to diminished hydrogen passivation efficiency, concurrently inhibiting graphitization

transformation and transfer film formation, thereby increasing the friction coefficient. Concurrently, the weakened interaction at the sliding interface reduces the wear rate, extending wear life. Nevertheless, the interplay between temperature, load, and environment complicates direct quantitative characterization of friction interfacial activity. Introducing the concept of interfacial activity offers a unified framework for qualitatively elucidating how these coupled effects jointly regulate friction evolution under cryogenic conditions.

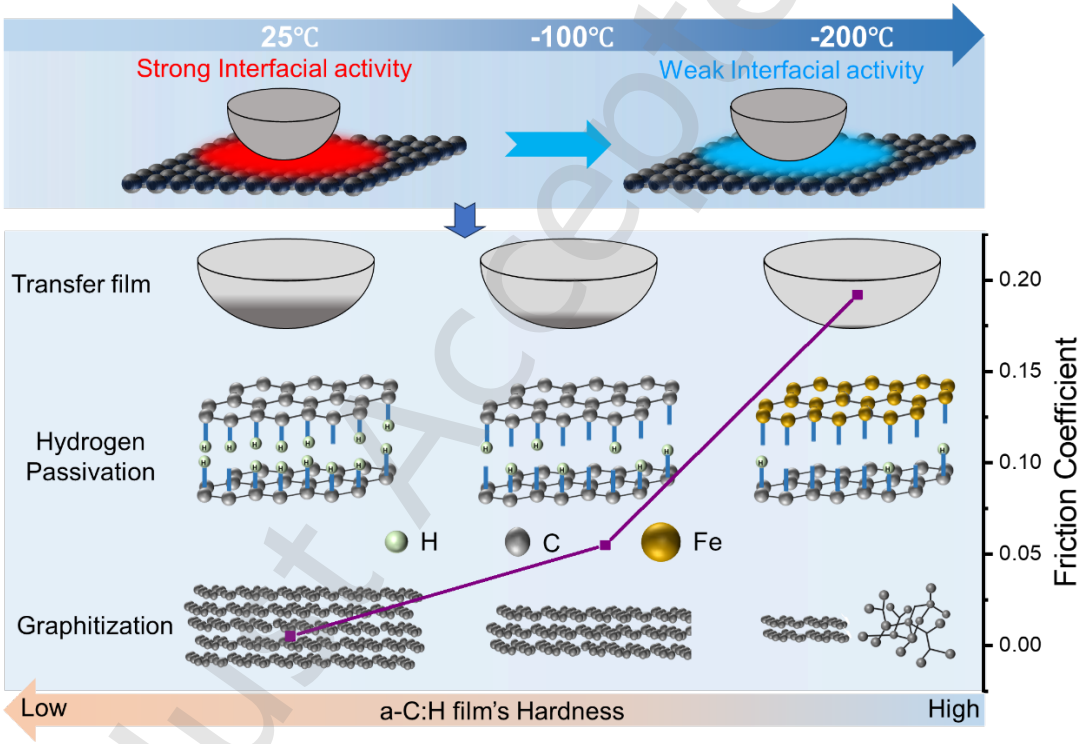


**Fig. 11.** Schematic diagram of the friction interface structure evolution of a-C:H films at cryogenic temperatures.

## 4. Conclusions

The interfacial activity governs the friction-wear trade-off for a-C:H films at cryogenic temperature. At room temperature, strong interfacial interactions between the GCr15 ball and a-C:H film drive massive carbon transfer to the ball, transforming the

friction interface from GCr15/a-C:H to a low-shear C/C contact. This transformation results in severe damage to the a-C:H film. The hydrogen generated during friction passivates highly reactive carbon dangling bonds and pronounced graphitization under frictional heating further reduces friction. However, this interface is unstable and requires continuous carbon replenishment, leading to a short wear life despite low friction at room temperature.

In contrast, at cryogenic temperatures, weak interfacial activity reduces the interaction strength between the GCr15 ball and a-C:H film. This change has two key effects. Firstly, it significantly inhibits carbon transfer to the ball, effectively reducing the a-C:H film's damage. Secondly, it weakens the collaborative lubrication of transfer films, hydrogen passivation, and graphitization. Consequently, a high friction coefficient coexists with a low wear rate at cryogenic temperatures. Additionally, the increased hardness of the a-C:H film at cryogenic temperatures reduces the contact area, further lowering its wear.

## Declaration of Competing Interest

The authors declare that they have no known competing financial interests or personal relationships that could have appeared to influence the work reported in this paper.

## Acknowledgments

The authors gratefully acknowledge the financial support of Strategic Priority Research Program of the Chinese Academy of Sciences (Grant No. XDB0470202), Key Program of the Lanzhou Institute of Chemical Physics, CAS (Grant No. KJZLZD-3),

National Natural Science Foundation of China (Grant No.52275222) and Key Science and Technology Program of Gansu Province (Grant No. 22ZD6GA002) and Longyuan Youth Talent Project.

## References

[1] Behnia K. The fragility of distant cooper pairs. *Science* **355** (6320): 26-27 (2017)

[2] Xie Z A, Jin Q H, Su G L, Lu W. A Review of hydrogen storage and transportation: Progresses and challenges. *Energies* **17** (16): 4070 (2024)

[3] Gu L, Wang L Q, Zheng D Z, Jia X M. Study on the characteristics of transferred lubricating thin films on ceramic surfaces generated in liquid nitrogen. *Tribol. Trans.* **53** (2): 161-168 (2010)

[4] Porfiryev Y, Shuvalov S, Popov P, Kolybelsky D, Petrova D, Ivanov E, Tonkonogov B, Vinokurov V. Effect of base oil nature on the operational properties of low-temperature greases. *Acs Omega* **5** (21): 11946-11954 (2020)

[5] Antonov S A, Bartko R V, Nikul'shin P A, Kilyakova A Y, Tonkonogov B P, Danilov A M. The current state of development of greases. *Chem Tech Fuels Oil*+ **57** (2): 279-288 (2021)

[6] Ren Y L, Zhang L, Xie G X, Li Z B, Chen H, Gong H J, Xu W H, Guo D, Luo J B. A review on tribology of polymer composite coatings. *Friction* **9** (3): 429-470 (2021)

[7] John M, Menezes P L. Self-lubricating materials for extreme condition applications. *Materials* **14** (19): 5588 (2021)

[8] Zhao B, Pan J W. Quantum control of reactions and collisions at ultralow

temperatures. *Chem. Soc. Rev.* **51** (5): 1685-1701 (2022)

[9] Hamilton M A, Alvarez L A, Mauntler N A, Argibay N, Colbert R, Burris D L, Muratore C, Voevodin A A, Perry S S, Sawyer W G. A possible link between macroscopic wear and temperature dependent friction behaviors of $MoS_2$ coatings. *Tribol. Lett.* **32** (2): 91-98 (2008)

[10] Liu H T, Ji H M, Wang X M. Tribological properties of ultra-high molecular weight polyethylene at ultra-low temperature. *Cryogenics* **58**: 1-4 (2013)

[11] Zhang G G, Sun Y L, Qian B K, Gao H, Zuo D W. Experimental study on mechanical performance of polydimethylsiloxane (PDMS) at various temperatures. *Polym. Test.* **90**: 106670 (2020)

[12] Ostrovskaya Y L, Yukhno T P, Gamulya G D, Vvedenskij Y V, Kuleba V I. Low temperature tribology at the B. Verkin Institute for low temperature physics & engineering (historical review). *Tribol. Int.* **34** (4): 265-276 (2001)

[13] Santos L V, Trava-Airoldi V J, Corat E J, Nogueira J, Leite N F. DLC cold welding prevention films on a Ti6Al4V alloy for space applications. *Surf. Coat. Technol.* **200** (8): 2587-2593 (2006)

[14] Chen D, Li J Z, Yuan Y H, Gao C, Cui Y G, Li S C, Liu X, Wang H Y, Peng C, Wu Z J. A review of the polymer for cryogenic application: methods, mechanisms and perspectives. *Polymers* **13** (3): 320 (2021)

[15] Cui W Y, Chen H Z, Zhao J X, Ma Q S, Xu Q, Ma T B. Progresses on cryo-tribology: lubrication mechanisms, detection methods and applications. *Int. J. Extreme Manuf.* **5** (2): 022004 (2023)

[16] de Mello J D B. Carbon-based solid lubricants: An overview. *Friction* **13** (1): 9441017 (2025)

[17] Fan X Q, Xue Q J, Wang L P. Carbon-based solid-liquid lubricating coatings for space applications-A review. *Friction* **3** (3): 191-207 (2015)

[18] Jang S, Chen Z, Kim S H. Origin of superlubricity of diamond-like carbon (DLC). *Friction* **13** (1): 9440995 (2025)

[19] Erdemir A, Nichols F A, Pan X Z, Wei R, Wilbur P. Friction and wear performance of ion-beam-deposited diamond-like carbon-films on steel substrates. *Diam. Relat. Mater.* **3** (1-2): 119-125 (1994)

[20] Yang Y L, Chen Y J, Han T Y, Shang L L, Liu B, Pan M H, Liang Y, Chen X. Evolution of interfacial nanostructures with temperature governing fretting wear in diamond-like carbon films. *Carbon* **226**: 119217 (2024)

[21] Khan M S, Sasikumar C. Diamond-like carbon/Cu composite films on stainless steel: synthesis and investigation of heat transfer properties. *J. Nanopart. Res.* **26** (3): 62 (2024)

[22] Wang C C, Song X, Shen X T, Sun F H. Molecular dynamics simulation and experimental investigation of structural transformation and graphitization in diamond during friction. *Comput. Mater. Sci.* **184**, 109862 (2020)

[23] Cui L C, Lu Z B, Wang L P. Probing the low-friction mechanism of diamond-like carbon by varying of sliding velocity and vacuum pressure. *Carbon* **66**: 259-266 (2014)

[24] Rabinowicz E. Friction and wear of materials. *Wiley.* New York 1965.

[25] Ma T B, Hu Y Z, Wang H. Molecular dynamics simulation of shear-induced graphitization of amorphous carbon films. *Carbon* **47** (8): 1953-1957 (2009)

[26] Fontaine J, Belin M, Le Mogne T, Grill A. How to restore superlow friction of DLC: the healing effect of hydrogen gas. *Tribol. Int.* **37** (11-12): 869-877 (2004)

[27] Jang S, Kim S H. Distinct effects of endogenous hydrogen content and exogenous hydrogen supply on superlubricity of diamond-like carbon. *Carbon* **202**: 61-69 (2023)

[28] Li X W, Wang A Y, Lee K R. Atomistic understanding on friction behavior of amorphous carbon films induced by surface hydrogenated modification. *Tribol. Int.* **136**: 446-454 (2019)

[29] Fontaine J, Donnet C, Grill A, LeMogne T. Tribochemistry between hydrogen and diamond-like carbon films. *Surf. Coat. Technol.* **146**: 286-291 (2001)

[30] Huang G W, Xue W L, Ren K X, Gao X C, Wang R C, Wang P, Gong Z B. Uncovering diamond-like carbon films super lubricity: From microscopic to macroscopic. *ACS Appl. Nano Mater.* **7** (20): 23981-23988 (2024)

[31] Wang K, Zhang J, Ma T B, Liu Y M, Song A, Chen X C, Hu Y Z, Carpick R W, Luo J B. Unraveling the friction evolution mechanism of diamond-like carbon film during nanoscale running-in process toward superlubricity. *Small* **17** (1): 2005607 (2021)

[32] Scharf T W, Prasad S V. Solid lubricants: A review. *J Mater Sci.* **48** (2): 511-531 (2013)